

A 2.4-7GHz Dual Band Microstrip Patch Antenna (DB-MPA)

Koyu Chinen¹, Shoko Nakamoto¹, Ichiko Kinjo²

¹GLEX, Yokohama, Japan

²National Institute of Technology, Okinawa College, Okinawa, Japan

Corresponding Author: Koyu Chinen

ABSTRACT

We designed a 2.4-7GHz dual-band microstrip patch antenna DB-MPA using electromagnetic field simulation and transmission characteristic (S21) measurements. Optimizing the slot length of the patch surface increased the directional antenna gain at 7 GHz by 3.5 dB compared to 2.48 GHz, reducing the effect of the higher spatial propagation loss of 9 dB at 7 GHz. A transmission system simulation with an antenna component model incorporating S21 data measured with the 2.4-7GHz DB-MPA from 1 to 8 GHz was conducted at a spatial propagation distance of 5 to 40 m to verify the practicality of the 2.4-7GHz DB-MPA.

KEYWORDS; DB-MPA; 2.4 and 7 GHz microstrip patch antenna; S21 design MPA; MPA transmission

Date of Submission: 24-09-2024

Date of acceptance: 06-10-2024

I. INTRODUCTION

The microstrip patch antennas (MPAs) are planar antennas consisting of a metal film radiation element (patch) formed on the surface of a dielectric substrate and a metal film ground on the backside. They have been widely studied because they are easy to design and manufacture. For example, MPAs have been studied to achieve a wide bandwidth by forming standard rectangular patch surfaces and slots [1-5]. Multi-band microstrip antennas with multiple frequencies (MB-MPA), two-frequencies (2.5, 3.5 GHz) [6], (2.396, 2.53 GHz) [7], (3.52, 6 GHz) [8], (2.4-2.73, 3.4-5.73 GHz) [9], three-frequencies (2.4, 3.7, and 4.7 GHz) [11], (2.45, 3.5, and 4.65 GHz) [10], four frequencies (7.2-17.5 GHz) [12], and five frequencies (5-12 GHz) [13] are in the study. There are also studies of antennas with different slot and patch surface geometries (2, 11 GHz) [14], (8.5 GHz) [15], (2.45 GHz) [16], and combined antennas with inversed F type antenna (IFAs) (5-6 GHz) [17]. Furthermore, there are reports of array antennas with multiple MPAs [18], [19]. Thus, multi-band MB-MPAs have been actively studied.

A mid-band frequency, 1 to 7.125 GHz as Sub-7GHz, will be used for 5G-advanced, so the two frequencies of 2.4 and 7 GHz are attractive in an antenna design for wireless fidelity (Wi-Fi) [20] and Sub-7GHz. In the dual band DB-MPA design for the two frequency bands of 2.4 GHz and 7 GHz, the difference in spatial propagation loss increases with the difference in the frequencies, so the gain of the DB-MPA at the high frequency needs to be improved. We designed a wide-range 2.4-7GHz dual-band MPA with an optimized of rectangular patch antenna slot length. Using electromagnetic field simulation, we analyzed the current density distribution on the patch surface and 3D electric field intensity radiation distribution. We conducted transmission and receiving system simulation using 2.4-7GHz DB-MPA and a vector network analyzer and investigated the possibility of long-distance communication (5 to 40 m).

II. 2.4 - 7GHz DUAL BAND MICROSTRIP PATCH ANTENNA (DB-MPA) DESIGN

We designed and fabricated a dual-band microstrip patch antenna (DB-MPA) for the 2.48 GHz and 7 GHz frequency bands. The substrate used was a 1.6 mm thick FR-4 glass epoxy dielectric substrate (60 × 60 mm) with 35 μm thick copper foil on both sides. As shown in Fig. 1, a patch of length (L_{MPA}) = 28 mm and width (W_{MPA}) = 37 mm was formed on the copper foil on the surface of the substrate, and a 50 Ω micro-stripped line (MSL) of 3 mm width was used to feed the patch. Two slots 8.5 mm long and 0.75 mm wide were formed on both sides of the microstrip line (MSL). The S-parameters (S_{11}) were obtained by an electromagnetic field simulator (AXIEM) [21] when the lengths of the slots L_s were varied from 6, 8.5, 10, and 15 mm. As shown in Fig. 2, resonant frequencies appeared at 2.45, 3.75, 6.2, and 7.047 GHz. The slot length that showed the minimum value of S_{11} in the two frequency bands of $f_1 = 2.48$ GHz and $f_2 = 7$ GHz was $L_s = 8.5$ mm.

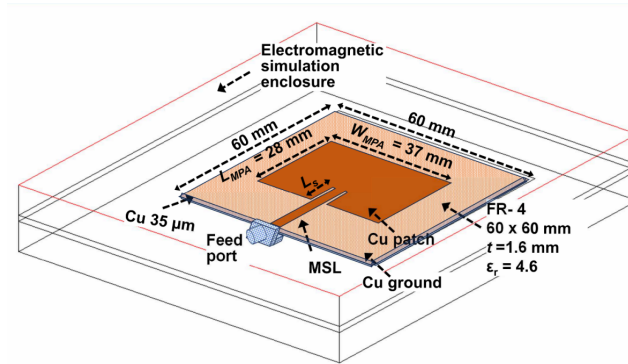


Figure 1: 2.4-7GHz dual-band microstrip patch antenna (DB-MPA) fabricated on FR-4 substrate.

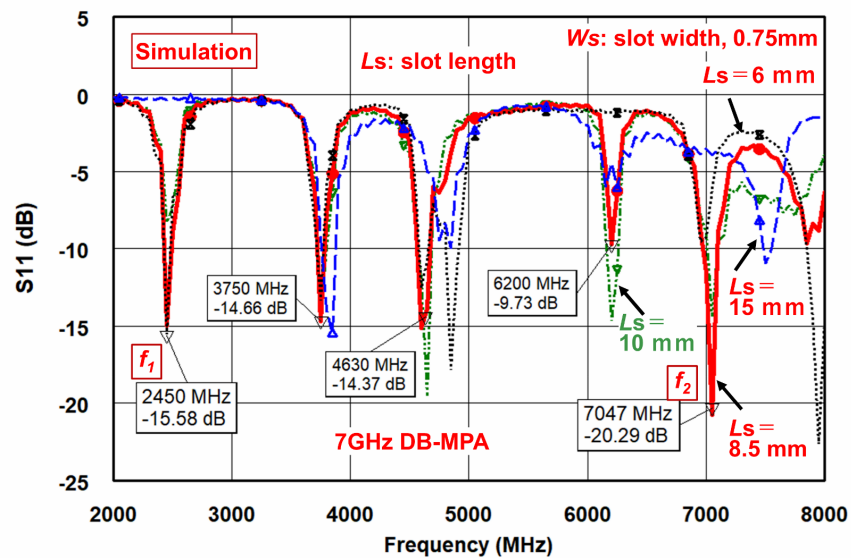


Figure 2: Reflective coefficient S-parameter S₁₁ simulated for 2.4-7GHz DB-MPA with different slot lengths L_s of 6, 8.5, 10, and 15 mm.

III. CURRENT DENSITY DISTRIBUTIONS AT THE 2.4-7GHz DUAL BAND PATCH ANTENNA

Using Maxwell's electromagnetic field equations and the *x-y-z* coordinates (Fig. 3), the θ -directional component dE_{θ} and the ϕ -directional component dE_{ϕ} of the radiated electric field intensity (dE) at distance r due to the current density (j) flowing over a small length (dx) of the patch antenna surface can be expressed as equations (1) and (2), respectively. In this equation, β is the wavenumber $2\pi/\lambda$, and η_0 is the spatial impedance .

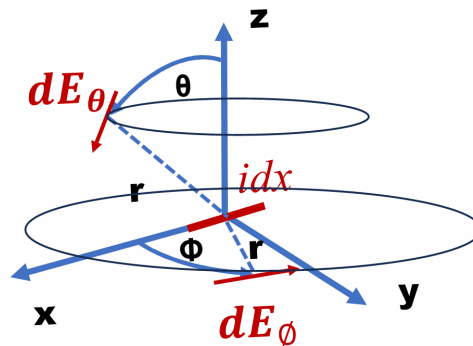


Figure 3: The current fragment jdx on the *x-y-z* coordinate origin point creates radiated electric field intensities dE_{θ} and dE_{ϕ} at a distance r from the origin point.

(1)

(2)

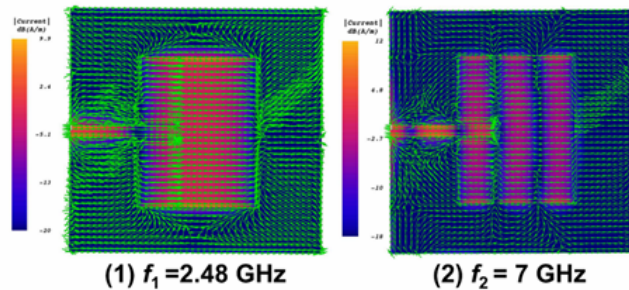


Figure 4: Current density distributions at 2.48 GHz and 7 GHz at the patch surface of 2.4-7GHz DB-MPA analyzed by electromagnetic field simulation.

The 3D electric field intensity patterns of E_θ and E_ϕ were obtained using the electromagnetic simulator AXIEM. The simulated $E_{\theta 1}$ and $E_{\phi 1}$ at the frequency $f_1 = 2.48$ GHz are shown in Fig. 4. The values of $E_{\theta 1}$ and $E_{\phi 1}$ vary with $\cos\theta$ and $\sin\phi$, respectively, which reflect the current direction of the patch antenna surface, as determined by (1) and (2). Equations (1) and (2) are complex numbers, but in this paper, simulated and calculated E_θ and E_ϕ values are expressed in terms of magnitude (absolute value).

Figure 5 shows the electrical field intensity patterns of $E_{\phi 1}$ and $E_{\theta 1}$ at a frequency of $f_1 = 2.48$ GHz, reflecting the current density distribution. The electrical field intensity patterns of $E_{\theta 2}$ and $E_{\phi 2}$ at a frequency of $f_2 = 7$ GHz are shown in Fig. 6. The field intensity pattern is sharper than at 2.48 GHz because the current density distribution shows a resonant mode in which the L_{MPA} is divided into three parts. The total power is expressed as $TP_{Wvr} = (E_\theta^2 + E_\phi^2)/(2\eta_0)$, which shows a hemispherical power distribution at 2.48 GHz, as shown in Fig. 7. At 7 GHz, the power distribution is slightly doughnut-shaped. A large power distribution on the substrate rear is considered to be because a part of the surface current return is located near the center of the patch surface.

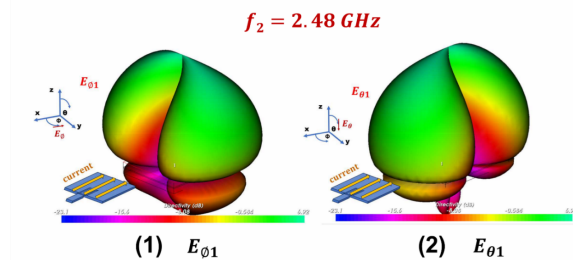


Figure 5: Electric field intensity $E_{\theta 1}$ and $E_{\phi 1}$ radiation patterns correspond to the current density distribution on the 2.4-7GHz DB-MPA patch surface at the frequency of 2.48 GHz.

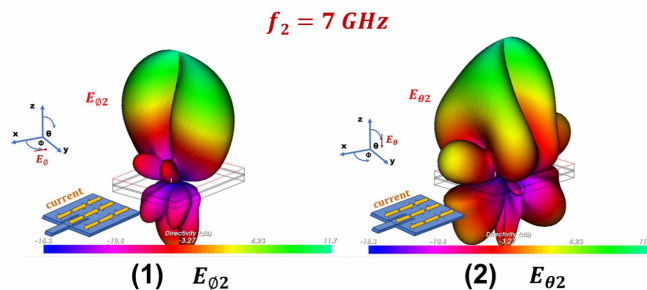


Figure 6: Electric field intensity $E_{\theta 2}$ and $E_{\phi 2}$ radiation patterns correspond to the current density distribution on the 2.4-7GHz DB-MPA patch surface at the frequency of 7 GHz.

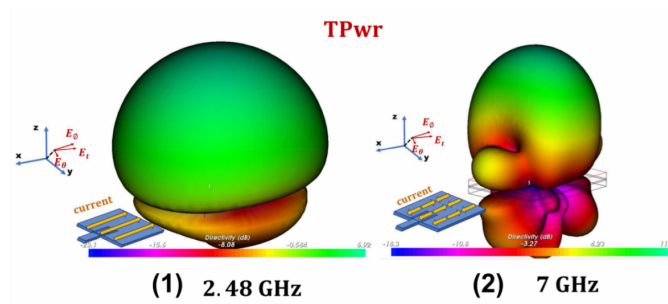


Figure 7: Total power $TPwr$ radiation patterns correspond to the current density distribution on the 2.4-7GHz DB-MPA patch surface at the frequency of 7 GHz.

IV. CROSS SECTIONAL VIEW OF ELECTRIC FIELD INTENSITY RADIATION FROM THE 2.4-7GHz DB-MPA

We investigated the 2D electric field intensity distributions of E_{θ} and E_{ϕ} at 2.48 GHz and 7 GHz resonant frequencies. The conic cuts of E_{θ} and E_{ϕ} at 2.48 GHz are shown in Fig. 8. The maximum value of the directional gain is 6.88 dBi ($\theta = 0^\circ$) at 2.48GHz. The gain value at $\theta = 30^\circ$ is close to $\theta = 0^\circ$. Since the E_{ϕ} is rotated 90 degrees from E_{θ} (see Fig.5), the gain value of E_{ϕ} is close to E_{θ} .

The maximum value of the directional gain is 11.7 dBi ($\theta = 0^\circ$) at 7 GHz, as shown in Fig. 9. The maximum gain values at $\theta = 30^\circ$ are 7.02 dB and 2.79 dB for $E_{\phi 2}$ and $E_{\theta 2}$, respectively. Since the electric field intensity radiation patterns of $E_{\phi 2}$ and $E_{\theta 2}$ are sharp and asymmetric (see Fig. 6), the directional gain is significantly increased when θ is increased.

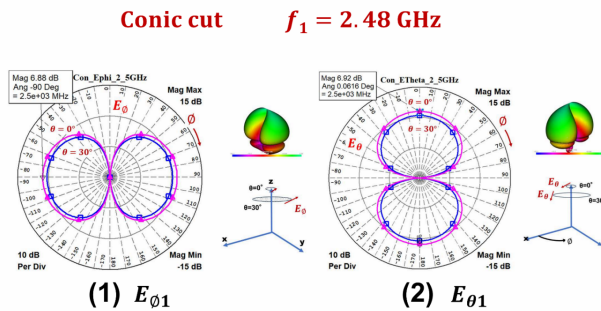


Figure 8: Conic cut cross sections at $\theta = 0^\circ$ and 30° of the electric field intensities $E_{\phi 1}$ and $E_{\theta 1}$ radiated from the current density distributions at frequency 2.48 GHz on the patch surface of the 2.4-7GHz DB-MPA.

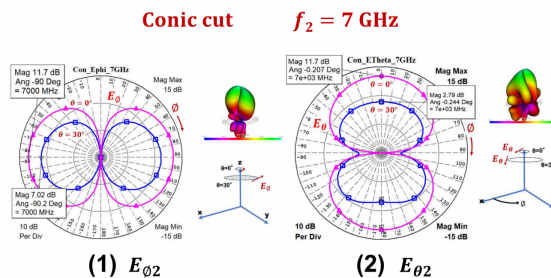


Figure 9: Conic cut cross sections at $\theta = 0^\circ$ and 30° of the electric field intensities $E_{\phi 2}$ and $E_{\theta 2}$ radiated from the current density distributions at frequency 7 GHz on the patch surface of the 2.4-7GHz DB-MPA.

Figure 10 shows the principal plane cuts of $E_{\theta 1}$ ($\varphi = 0^\circ$) and $E_{\phi 1}$ ($\varphi = 90^\circ$) at frequency $f_1 = 2.48$ GHz. The hemispherical distribution on the substrate surface reflects the electric field intensity radiation pattern (see Fig. 5). The maximum value of the directional gain is 6.92 dBi for $E_{\phi 1}$ and $E_{\theta 1}$.

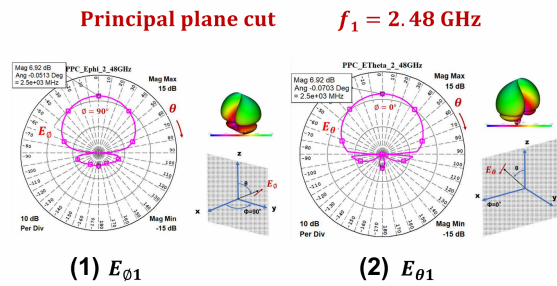


Figure 10: The principal plane cut cross sections at $\varphi = 90^\circ$ and 0° of the electric field intensities $E_{\phi 1}$ and $E_{\theta 1}$ radiated from the current density distributions at frequency 2.48 GHz on the patch surface of the 2.4-7GHz DB-MPA.

The principal plane cuts of $E_{\theta 2}$ ($\varphi = 0^\circ$) and $E_{\phi 2}$ ($\varphi = 90^\circ$) at frequency $f_2 = 7$ GHz are shown in Fig. 11. The maximum value of the directional gain is 11.7 dBi for $E_{\phi 2}$ and $E_{\theta 2}$. A sharpened and asymmetric intensity pattern is observed on the surface of the substrate, and a small radiation pattern is seen on the substrate's rear, reflecting the electric field intensity radiation pattern. The $TPwr$ conic cut distributions at 2.48 GHz and 7 GHz are shown in Fig. 12. The 2.48 GHz $TPwr$ shows a circle radiation distribution, and the 7 GHz $TPwr$ shows a little asymmetric distribution. The maximum directional gain is 6.92 dBi and 11.7 dBi for 2.48 GHz and 7 GHz, respectively. The sharpened electric field intensity radiation created by three resonant current sections realizes higher directional gain at 7 GHz than 2.4 GHz for the 2.4-7GHz DB-MPA.

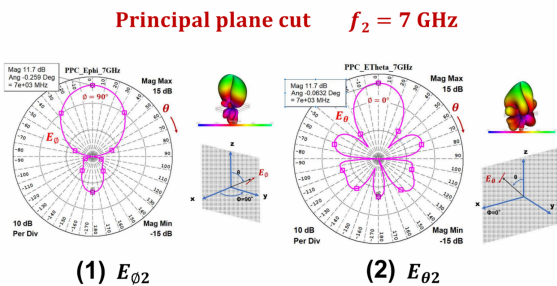


Figure 11: The principal plane cut cross sections at $\varphi = 90^\circ$ and 0° of the electric field intensities $E_{\phi 2}$ and $E_{\theta 2}$ radiated from the current density distributions at frequency 7 GHz on the patch surface of the 2.4-7GHz DB-MPA.

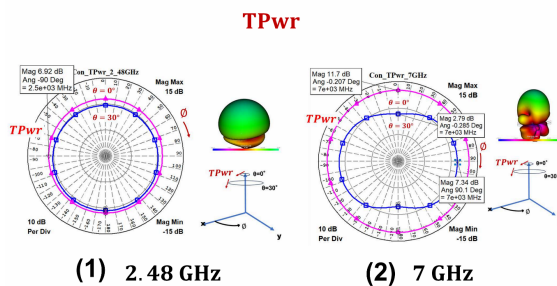


Figure 12: Conic cut cross sections of the total powers radiated from the current density distributions at frequencies 2.48 GHz and 7 GHz on the patch surface of the 2.4-7GHz DB-MPA.

We simulated the directional gain with the sweep frequency of the 2.4-7GHz DB-MPA using AXIEM. The directional gains of the E_ϕ at $\theta = 0^\circ$ and $\phi = 90^\circ$ and E_θ at $\theta = 0^\circ$ and $\phi = 0^\circ$ were plotted with frequencies from 2000 to 8000 MHz, as shown in Fig.13. The directional gains of E_θ ($\theta = 0^\circ$, $\phi = 0^\circ$) and E_ϕ ($\theta = 0^\circ$, $\phi = 90^\circ$) are the same. The directional gains at 2.5 GHz and 7 GHz were 6.916 dBi and 11.73 dBi, respectively. These values were the same as the maximum values obtained in Fig. 8-11.

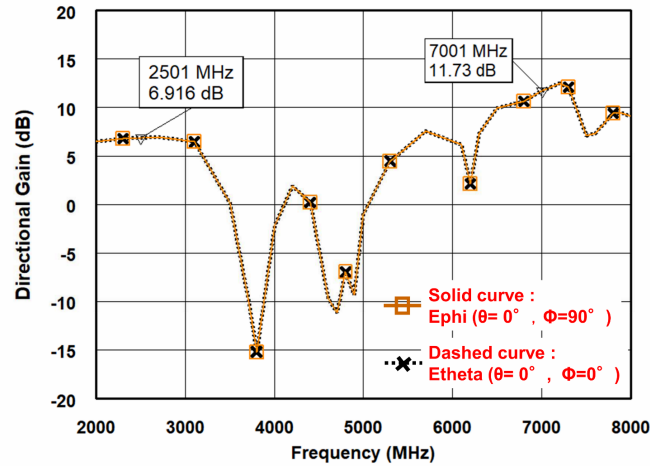


Figure 13: Simulated result of the directional gains of E_ϕ at $\theta = 0^\circ$ and $\phi = 90^\circ$ and E_θ at $\theta = 0^\circ$ and $\phi = 0^\circ$ with frequency sweep for the 2.4-7GHz DB-MPA.

V. MEASUREMENTS OF TRANSMISSION CHARACTERISTICS (S21) WITH TRANSMITTING AND RECEIVING ANTENNAS OF 2.47-7GHz DB-MPA

The reflection coefficient S_{11} and transmission coefficient S_{21} of the S-parameters from 1 to 8 GHz were measured by a vector network analyzer (VNA) using the fabricated 2.4-7GHz DB-MPA. The spatial propagation distance d_s between the transmitting antenna (TxMPA, DB-MPA) and the receiving antenna (RxMPA, DB-MPA) were set to 0.1 m, and the transmitting coefficient S_{21} was measured. The S-parameters S_{11} and S_{21} are shown in Fig. 14 and 15, and the S_{21} (-19 dB) measured at 7 GHz is 5 dB lower than the S_{21} (-14 dB) measured at 2.48 GHz.

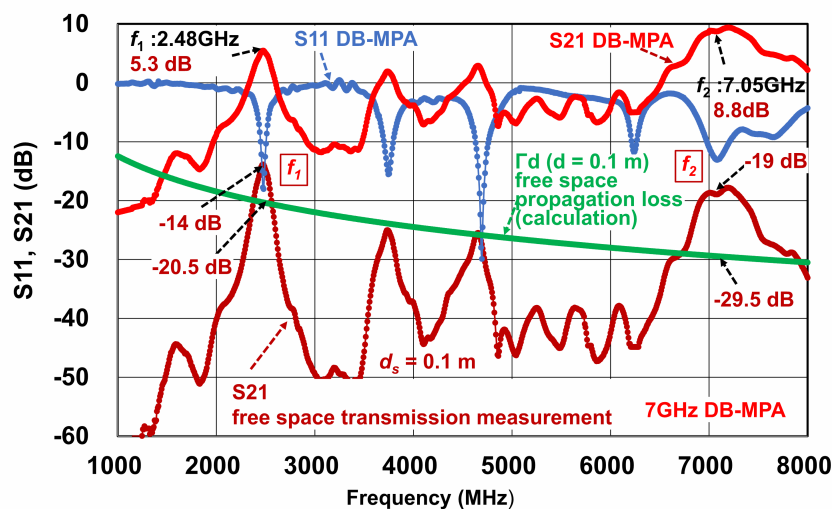


Figure 14: Reflection coefficient S_{11} and transmitting coefficient S_{21} measured with a vector network analyzer using 2.4-7GHz DB-MPA as the transmitting and receiving antennas (TxPMA and RxMPA). Calculated spatial propagation loss in the frequency range 0.1-8 GHz at a spatial propagation distance $d_s=0.1$ m.

The difference in S_{21} is due to the wavelength dependence of the spatial propagation loss Γ_d , as the calculated $\Gamma_{d=0.1m} = 29.5$ dB at $f_2 = 7$ GHz is 9 dB larger than the $\Gamma_{d=0.1m} = 20.5$ dB at 4.8 GHz. Considering the frequency dependence of the spatial propagation loss and the electrical connection loss, the S_{21} of the 2.4-7GHz DB-MPA alone is calculated to be 8.8 dB at 7 GHz and 5.3 dB at 2.48 GHz. The electromagnetic simulations of the cross cuts of the field intensity patterns, shown in Fig. 8 to 11, show the maximum directional gain of 11.7 dBi at 7 GHz and 6.9 dBi at 2.48 GHz, respectively. The cause of this difference between the S_{21} and directional gain can be attributed to the reflection of electromagnetic waves on the antenna surface and the gain distribution due to the polarization angle in the S_{21} measurement.

For a resonant frequency around 7 GHz, the resonant length is non-uniformly distributed in the L and W directions in the current density distribution in the L_{MPAe} , divided into three parts, as shown in Fig. 3(2).

The rectangular resonant frequency f_{mn} is represented by equation (3), which is derived from the cutoff resonant condition of $(\omega/C)^2 = k_m^2 + k_n^2$, where C is the light velocity, k_{mn} is the wavenumber, ϵ_r is the relative permittivity, L_{MPAe} and W_{MPAe} are the effective resonant lengths of the patch antenna, and the resonant mode orders m and n are integers.

(3)

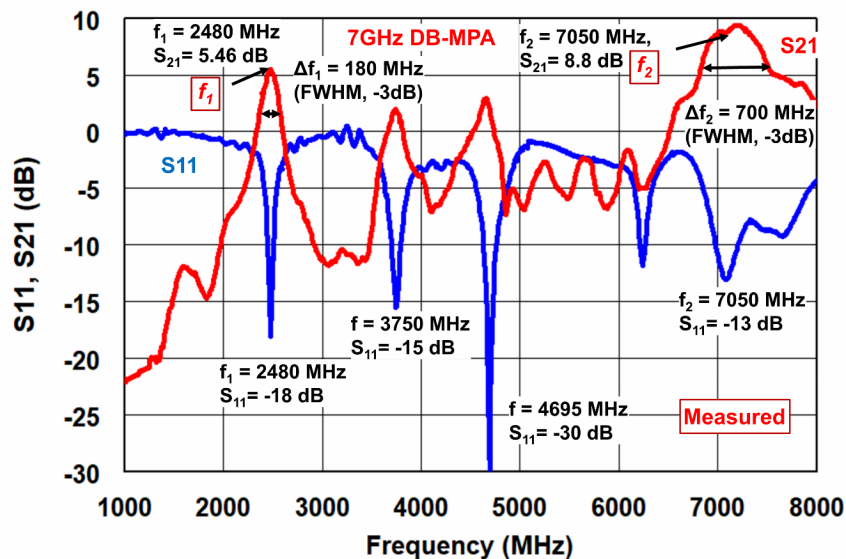


Figure 15: 2.4-7GHz DB-MPA reflection coefficient S_{11} , transmitting coefficient S_{21} , and -3 dB frequency bandwidth at S_{21} .

Figure 15 shows the details of S_{11} and S_{21} of 2.4-7GHz DB-MPA. The symbol f_1 shows a center frequency of 2.48 GHz, the resonant frequency bandwidth BW , full width at half maximum point (FWHM, -3dB), is 0.18 GHz, and $S_{21} = 5.46$ dB, while f_2 shows a center frequency of 7.05 GHz, a resonant BW of 0.7 GHz, and $S_{21} = 8.8$ dB. The three-part division in the current density distribution at around 7 GHz varies the effective resonant current length L_{MPAe} by interaction with the edge of the slots. When the effective resonant length L_{MPAe} varies from 30.8 to 28.0 mm and $m = 3$ and $n = 0$ in (3), the frequency f_{mn} varies from 6.8 to 7.5 GHz. The variation in the three-part resonant current modes causes a wide BW of 0.7 GHz at the resonant frequency of 7 GHz for 2.3-7GHz DB-MPA.

If we increase the resonant frequency higher than 7.5 GHz, the current density distribution changes to four modes, as shown in Fig. 16. The four-current mode resonant frequency f_{04} is calculated by (3) using $m = 0$, $n = 4$, and $W_{MPAe} = 37.3$ mm. This DB-MPA can be used for another application.

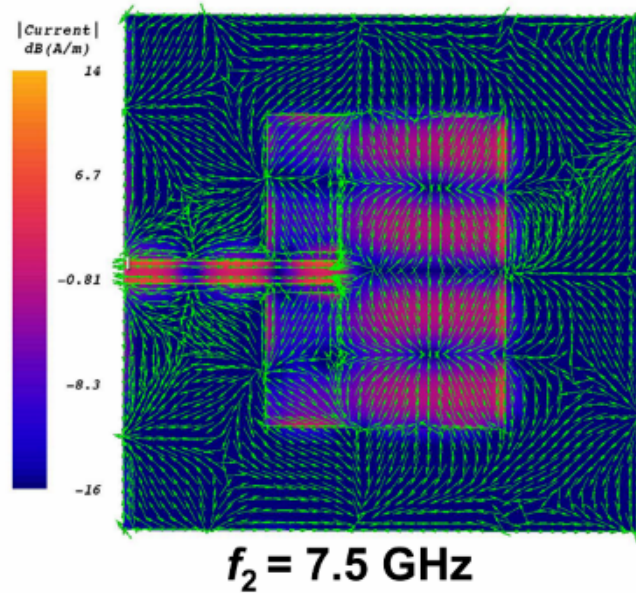


Figure 16: Current density distribution at frequency 7.5 GHz.

In addition to f_1 and f_2 , resonant frequencies at 3750 MHz ($S_{11} = -15\text{dB}$) and 4695 MHz ($S_{11} = -30\text{dB}$) appear in the 2.4-7 GHz DB-MPA, but the corresponding S_{21} is low as 1.91dB and 2.91dB, respectively. There is no strong correlation between S_{11} and S_{21} . Therefore, simulation of current density distribution, electrical field intensity pattern, and S_{21} measurements are essential in the design of S_{21} for MPA.

VI. TRANSMISSION COEFFICIENT S_{21} MEASUREMENTS WITH 2.7-7GHZ DB-MPA

A transmission system simulator (VSS) [20] was used to analyze the transmission characteristics of the system configuration using the 2.4-7GHz DB-MPA, as shown in Fig. 17. The component model of the 2.4-7GHz DB-MPA consists of the S-parameters S_{21} file PAS21 calculated from the experimental data measured at a spatial propagation distance of $d_s = 0.1$ m using the transmission and receiving antennas TxMPA and RxMPA. The spatial propagation distance d_s is incorporated into the component parameters of the receive antenna RxMPA.

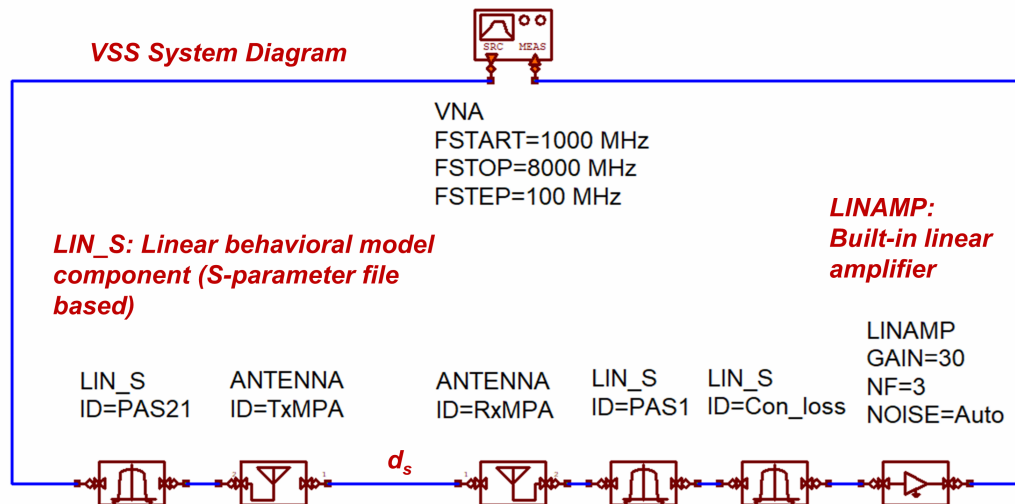


Figure 17: Transmission system simulation configuration using 2.4-7GHz DB-MPA as transmitter and receiver antennas.

Figure 18 shows the measured and simulated S_{21} transmission characteristics at spatial propagation distances of $d_s = 0.1$ m and 0.2 m for a transmission system configuration using 2.4-7GHz DB-MPA with receiving and transmitting antennas TxMPA and RxMPA. The measured and simulated values are almost the same, and the difference in S_{21} between $d_s = 0.1$ and 0.2 m at 7 GHz is nearly the same as the spatial propagation loss (about 6 dB). The simulated S_{21} at $d_s = 0.2$ m is almost equal to the measured value.

A system simulation was conducted by connecting a 30 dB linear amplifier LINAMP to the rear stage of the RxMPA to investigate the transmission characteristics at long spatial propagation distances of $d_s = 3, 10,$ and 40 m. The simulation results are shown in Fig. 19. Since a receiver power higher than -70 dBm is considered to be a practical signal level for digitally modulated wireless communication systems such as Wi-Fi and 6G, long-distance communication at 2.48 GHz and 7 GHz using the designed 2.4-7GHz DB-MPA is feasible.

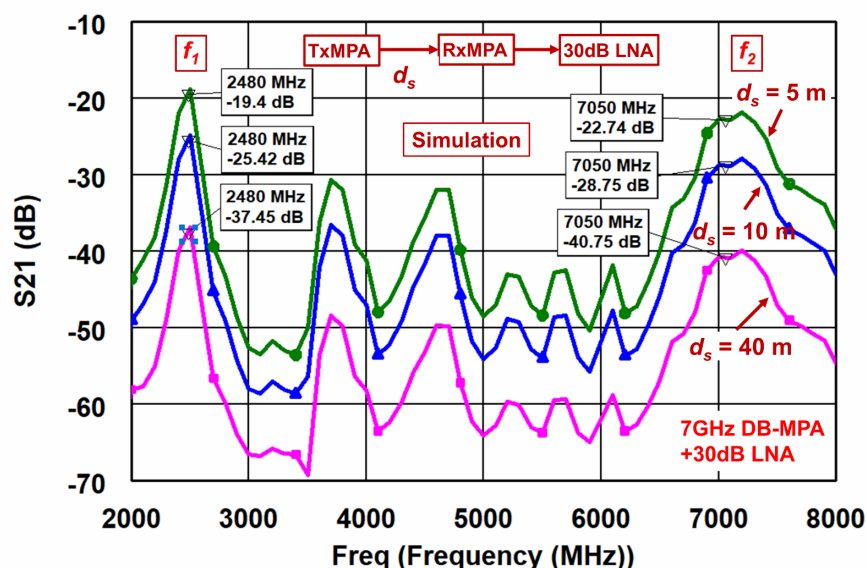


Figure 18: Measured (solid line) and simulated (dashed line) transmission characteristics (S_{21}) at spatial propagation distances $d_s = 0.1$ and 0.2 m using 2.4-7GHz DB-MPA as transmitting and receiving antennas (TxMP and RxMP).

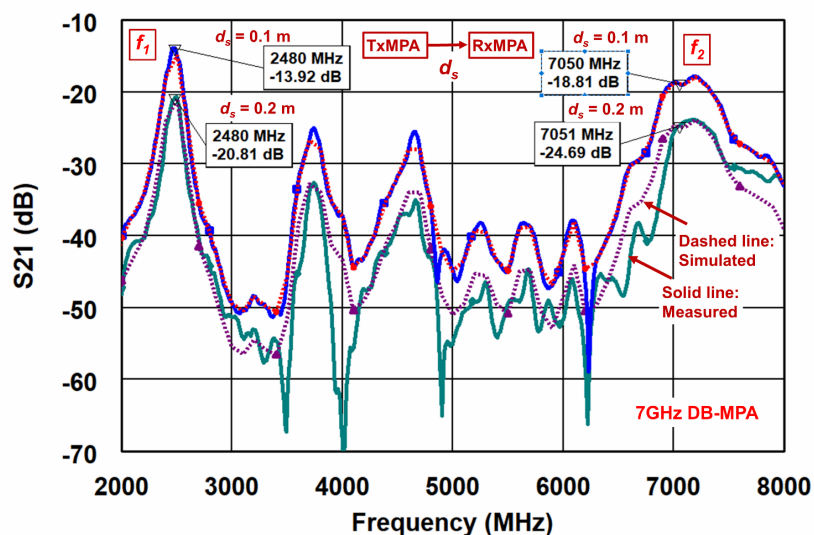


Figure 19: System simulation results of long-range transmission characteristics (S_{21}) using 2.4-7GHz DB-MPA as transmitting and receiving antennas (TxMP, RxMP) with spatial propagation distances $d_s =$

5, 10, and 40 m. A 30dB linear amplifier was connected at the rear of the receiving antenna (RxMPA).

VII. CONCLUSION

Using an electromagnetic field simulator we designed a 2.4-7 GHz dual-band microstrip patch antenna (DB-MPA), and fabricated it using an FR-4 substrate (35 μm copper foil thickness, 1.6 mm dielectric board thickness, relative permittivity). The minimum frequency reflection coefficient S_{11} was determined by optimizing the slot lengths at both sides of the electrical feed line MSL on the rectangular patch surfaces ($L_{\text{MSP}} \times W_{\text{MSP}}$). The current density distribution at 7 GHz showed a square resonant mode ($m = 3, n = 0$) with the L_{MSP} divided into three parts. The electric field intensity radiation distribution at 7 GHz showed a more acute shape than the resonant mode at 2.48 GHz ($m=1, n=0$), although the polarization direction was the same. The maximum directional gains at 2.48 GHz and 7 GHz obtained from the cross-sectional pattern of the electric field intensity radiation distribution were 6.92 dBi and 11.7 dBi, respectively. We also achieved these values from the simulation of the E_{θ} and E_{ϕ} with the frequency sweep. The transmitting coefficient S_{21} was measured using the fabricated 2.4-7GHz DB-MPA as the transmitter and receiver antennas. At a spatial propagation distance of $d_s = 0.1$ m, the transmission coefficients S_{21} at 2.48 GHz and 7 GHz were -14 dB and -19 dB, respectively.

Considering the difference of 9 dB in space propagation loss and 3 dB in total coaxial cable and adapter losses between 2.48 GHz and 7 GHz, the designed 2.4-7GHz DB-MPA has a directional gain of 5.46 dBi and 8.8 dBi at 2.48GHz and 7 GHz, respectively. The space propagation and coaxial cable and adapter losses are significant in wireless communications with a high-frequency difference. The S_{11} and S_{21} values of the MPA do not generally correlate well, so it is essential to evaluate the current density distribution, electric field intensity radiation pattern, and S_{21} values in the design of the 2.4-7GHz DB-MPA. A wireless system simulation shows that the transmitter and receiver using 2.4-7GHz DB-MPAs designed in this study can communicate at 2.48 GHz and 7 GHz with spatial propagation distances of $d_s = 5$ to 40 m.

REFERENCE

- [1]. Y. Wang and Y. Lu, "The Strip-Ground Rectangular Patch Antenna," Hindawi International Journal of Antennas and Propagation, vol. 2017, Article ID 5924157, 7 pages, 2017. <https://doi.org/10.1155/2017/5924157>
- [2]. N. Hussain, U. Azimov, M. Jeong, S. Rhee, S. W. Lee, and N. Kim, "A High-Gain Microstrip Patch Antenna Using Multiple Dielectric Superstrates for WLAN Applications," The Applied Computational Electromagnetics Society Journal (ACES), vol. 35, no. 2, pp. 87-193, 2020.
- [3]. R. V. Gatti, R. Rossi, M. Dionigi, "Single-Layer Line-Fed Broadband Microstrip Patch Antenna on Thin Substrates," Electronics 2021, 10, 37, 2021. <https://doi.org/10.3390/electronics10010037>
- [4]. S. Rana, K. Sen, T. Mamun, S. Mahmud, M. Rahman, "A 2.45 GHz microstrip patch antenna design, simulation, and analysis for wireless applications," Bulletin of Electrical Engineering and Informatics, vol. 12, no. 4, August 2023, pp. 2173-2184, ISSN: 2302-9285, <https://doi.org/10.11591/eei.v12i4.4770>
- [5]. S. Rana, H.O. Rasid, S. K. S. Shuva, S. Ahmed, S. R. Islam, M. Rahman, "Design, Simulation and Analysis of 3.5 GHz Microstrip Patch Antenna for Wireless Communication Systems," 4th ICCNT IEEE Conference Jul 6-8, Delhi, Conference Paper, July 2023, <https://doi.org/10.1109/ICCCNT56998.2023.10307552>
- [6]. I. Ali, and R. Y. Chang, "Design of Dual-Band Microstrip Patch Antenna with Defected Ground Plane for Modern Wireless Applications," 2015 IEEE 82nd Vehicular Technology Conference (VTC2015-Fall), 06-09 September, 2015. <https://doi.org/10.1109/VTCFall.2015.7390887>
- [7]. H. Normikman, B. H. Ahmad, M. Z. A. Abd Aziz, H. A. Bakar, "Dual Frequencies Band and Enhanced Wideband Effect of Dual Layer Microstrip Patch Antenna with Parasitic," IOP Conf. Series: Journal of Physics: Conf. Serie 1049 (2018) 012012, 2018. <https://doi.org/10.1088/1742-6596/1049/1/012012>
- [8]. S. K. Noor, M. Jusoh, T. Sabapathy, A.H. Rambe, H. Vettikalladi, A. M. Albishi, Himdi, "A Patch Antenna with Enhanced Gain and Bandwidth for Sub-6 GHz and Sub-7 GHz 5G Wireless Applications," Electronics 2023, 12, 2555, 2023. <https://doi.org/10.3390/electronics12122555>
- [9]. M. Bikrat, S. Bri, A. G Bravo, A. M. Manterola, M. Gonzalez-Atienza, F. A. Amador, "Multi-Bandwidth Reconfigurable Patch Antenna for Devices in WLAN and UWB Technology Applications," Appl. Sci. 13, 9367, 2023. <https://doi.org/10.3390/app13169367>
- [10]. Pragati, S.L. Tripathi, S. R. Patre, S. Singh and S.P. Singh, "Triple-band Microstrip Patch Antenna with Improved Gain," International Conference on Emerging Trends in Electrical, Electronics and Sustainable Energy Systems (ICETESES-16), pp. 106-110, Feb. 2016.
- [11]. Ossa-Molina, F. Lopez-Giraldo, "A Simple Model to Compute the Characteristic Parameters of a Slotted Rectangular Microstrip Patch Antenna," Electronics 2022, 11, 129, 2022. <https://doi.org/10.3390/electronics11010129>
- [12]. M. A. Layegh, C. Ghobadi and J. Nourinia, "The Optimization Design of a Novel Slotted Microstrip Patch Antenna with Multi-Bands Using Adaptive Network-Based Fuzzy Inference System," Technologies 2017, 5, 75, 2017. 10. <https://doi.org/10.3390/technologies5040075>
- [13]. Ahmad, G.O. Lee, D. y. Choi, "Design and Performance Evaluation of a Compact Frequency Reconfigurable Coplanar-Waveguide-Fed Slotted Patch Antenna for Multi-Band Wireless Communication," Electronics 2023, 12, 3889, 2023. <https://doi.org/10.3390/electronics12183889>
- [14]. Y. Rhazi, O. E. Bakkali, Y. E. merabet, M. A. lafkih, S. Bri, M. N. Srifi, "Novel Design of Multiband Microstrip Patch Antenna for Wireless Communication," Advances in Science, Technology and Engineering Systems Journal, vol. 4, no. 3, pp. 63-68, 2019. <https://doi.org/10.25046/aj040310>

- [15]. M. Sharafeldin A. Boush, C. Kaur, "A Design for the Bandwidth Improvement for the Microstrip Patch Antenna for Wireless Network Sensor," International Journal of Scientific Research in Science, Engineering and Technology, Online ISSN: 2394-4099, 2022, <https://doi.org/10.32628/IJSRSET2293130>
- [16]. N. Markad, S. Mahadik, "Broadband circular polarized patch antenna with harmonic suppression," Indian Journal of Science and Technology 13(38): 4073-4083, 2020. <https://doi.org/10.17485/IJST/v13i38.1682>
- [17]. X.-P. Li, Q.M. Zhang, L. Yan, C. Q. Wang, W. Li, "A Double-Layer Patch Antenna for 5–6 GHz Wireless Communication," Micromachines 2022, 13, 929, 2022. <https://doi.org/10.3390/mi13060929>
- [18]. L. C. Paul, I. Hasan, R. Azim, R. Islam, M. T. Islam, "Design of High Gain Microstrip Array Antenna and Beam Steering for X Band RADAR Application," Joint 9th International Conference on Informatics, Electronics & Vision (ICIEV) and 2020 4th International Conference on Imaging, Vision & Pattern Recognition (icIVPR), 2020. <https://doi.org/10.1109/ICIEVicIVPR48672.2020.9306519>
- [19]. D.A. Jimenez, A. Reyna, L.I. Balderas, M.A. Panduro, "Design of 4×4 Low-Profile Antenna Array for CubeSat Applications," Micromachines 2023, 14, 180. <https://doi.org/10.3390/mi14010180>
- [20]. <https://www.wi-fi.org>
- [21]. https://www.cadence.com/en_US/home/tools/system-analysis/rf-microwave-design/awr-microwave-office.html